Int. J. Electrochem. Sci., 16 **(2021)** Article Number: 211013, doi: 10.20964/2021.10.04

International Journal of
ELECTROCHEMICAL
SCIENCE
www.electrochemsci.org

Synthesis of Carbon coated Silicon Monoxide with double carbon source and its application as anode for Lithium Ion Battery

Wang Li[*], *Lan Zhou, Wenjun Liao*

Central Academe, Shanghai Electric Group Co., Ltd. Shanghai 200070, China
[*]E-mail: 361377505@qq.com

Received: 3 June 2021 / *Accepted:* 19 July 2021 / *Published:* 10 September 2021

The low initial coulombic efficiency and poor cycling performance of commercial SiO limits its large-scale business application. The initial coulombic efficiency was increased and the cycling performance was improved significantly of commercial SiO by coated vitamin C and carbon nanotubes heated to 950℃. The prepared SiO/C/CNTs-2 delivered excellent performance, which are an initial charge-discharge efficiency of 74.1%, a high reversible capacity of 1335 mAh/g and a high retention rate of 96.9% after 120 cycles, and an low average cycle capacity loss of 0.36 mAh/g. However, the initial charge-discharge of uncoated commercial SiO is 70.6%, the capacity retention rate is 63.1% after 20 cycles, and the average cycle capacity loss is 29.6 mAh/g. Compared with uncoated commercial SiO, there is significant improvement in application as anode for lithium ion battery.

Keywords: Lithium-ion battery, Anode material, Silicon monoxide, Carbon coating, Carbon nanotubes

1. INTRODUCTION

The increasing use of petrochemical resources and the accumulation of greenhouse gases accelerate the global warming rate. In October 2018, the United Nations Panel on Climate Change issued a report calling all countries to take action to keep the temperature below 1.5℃. At the 75th session of the UN General Assembly, the Chinese government proposed that China will increase its nationally determined contributions, adopt more effective policies and measures, striving to peak its carbon dioxide emissions by 2030, and to achieve carbon neutrality by 2060.

The emergence of commercial lithium-ion batteries has accelerated the transformation of the automobile industry from fuel to electric, which makes the wind-solar energy storage power station

with reliable economic benefits, greatly reduces the phenomenon of wind and light abandonment, and at the same time provides a large amount of green energy. Range anxiety has always been a problem perplexing enterprises and consumers. This problem can only be effectively alleviated by improving battery design and increasing the capacity of positive and negative electrode materials. At present, most commercial lithium-ion batteries use graphite as the negative electrode, with a theoretical capacity of 372 mAh/g at room temperature [1], which is difficult to meet the demand of large-capacity batteries. The theoretical capacity of silicon is as high as 3579 mAh/g, and low lithium insertion voltage (~0.4 V versus Li^+/Li), which is regarded as next-generation anode materials. However, silicon undergoes a huge volume change (around 280%) during the lithium/delithuim process, which directly results in a serious decline in electrochemical performance [2-4]. As the anode material of lithium-ion batteries, relevant reports of silicon monoxide have been reported in the early stage [5]. The initial lithium intercalation capacity of silicon monoxide is 2400-2700 mAh/g, the volume expands 200% after discharge, the delithium capacity is 1300-1500 mAh/g, and the initial coulombic efficiency is about 50%[6]. The low initial charge -discharge efficiency and poor cycle performance limit the commercial application of silicon monoxide. The appeal problem can be effectively alleviated by nano-sized [7,8], alloying [9-13], porous [14,15], surface modification [16,17], development of new binder and electrolyte additive [18-21]. In this paper, the surface of silicon monoxide was modified by the method of double carbon source coating, which not only increased initial charge-discharge efficiency but also significantly improved the cycling performance of silicon monoxide.

2. EXPERIMENTAL

2.1 Materials synthesis

With the commercial SiO as raw material, vitamin C and carbon nanotubes as carbon source, and deionized water as solvent, according to mass ratio 25% vitamin C was firstly weighted and dissolved in an appropriate amount of deionized water, secondly then 0%, 0.2% and 0.5% carbon nanotubes were weighted and added to the solution respectively, and last SiO was added to the above solution with ultrasonic for 15min. The composite precursors were prepared after spray drying that were placed in a tube furnace heated to 950℃ for 4 h in argon atmosphere, and then cooled to room temperature. The composite materials were marked as SiO/C, SiO/C/CNTs-1 and SiO/C/CNTs-2, respectively. Untreated commercial SiO was labeled as SiO.

2.2 Materials characterization

Specific surface area of the samples were calculated by using the Brunauer- Emmett- Teller (BET) mode and performed on Gemini VII (Micromeritics Instrument Corp., USA). Raman spectrum was tested by LabRAM HR Evolution(HORIBA Scientific Corp., France). The morphology of nano-silicon powders were observed by filed emission scanning electron microscope (FE-SEM, Sigma 500, Zeiss).The crystalline structures of samples were measured by X-ray diffraction (XRD,

6100,Shimadzu) with Cu Kα radiation at a scanning rate of 2°/min in a reflection mode over a 2θ ranging from 10° to 90°.

2.3 Electrochemical test

The working electrodes were prepared by a slurry uniformly coated onto the copper foil, including 60wt% active material, 20wt% Super P, 8wt% CMC and 12wt% SBR dissolved in deionized water. The electrodes were dried in oven at 50°C for 5 min and then in vacuum 90°C for 12 h. The mass loading of the active material on the working electrodes was ~1.1 mg cm^{-2}.The electrochemical performances of nano-silicon powder were tested in CR2032 coin-type cells. Coin cells were assembled in a glove box full of argon (LABstar, MBRAUN Co., Ltd., China) using Li foil as the counter/reference electrode, Celgard 2400 as a separator and 1M $LiPF_6$ in ethylene carbonate/ dimethyl carbonate (EC/DMC, 1:1 by volume) with 1 wt% vinyl carbonate (VC) and 10 wt% fluoroethylene carbonate (FEC) additives as the electrolyte. Before the test, coin cells were placed at room temperature for 12 h. LAND 2013A battery tester was used for galvanostatic measurements. The charge and discharge procedures in this paper as followed: 0.1C charge and discharge cycle was set as gradient discharge 0.1 C to 5 mv, 0.05 C to 5 mv, 0.02 C to 5 mv, and then charge 0.1 C to 2 v. 0.5 C charge and discharge cycle was set as gradient discharge 0.5 C to 5 mv, 0.2 C to 5 mv, 0.1 C to 5 mv, 0.05 C to 5 mv, 0.02 C to 5 mv, and then charge 0.5 C to 2 v, 1 C=1700 mA/g.

3. RESULTS AND DISCUSSION

Fig. 1 SEM observations show that the surface morphology of different samples. The SiO presents an angular blocks with a large number of fine particles distributing on the surface. The coating process of vitamin C and carbon nanotubes changes the surface morphology of SiO and reduce the number of fine particles on the surface. Scanning electron microscopy images of SiO/C/CNTs-1 and SiO/C/CNTs-2 show that carbon nanotubes and amorphous carbon are uniformly distributed on the surface and between the particles of SiO, which could effectively alleviate the electrode stripping reaction caused by materials volume changes in the process of lithiation/delithiation, and at the same time, an excellent conductive network is constructed to enhance the electron transport capacity. It is beneficial to play full capacity for active materials.

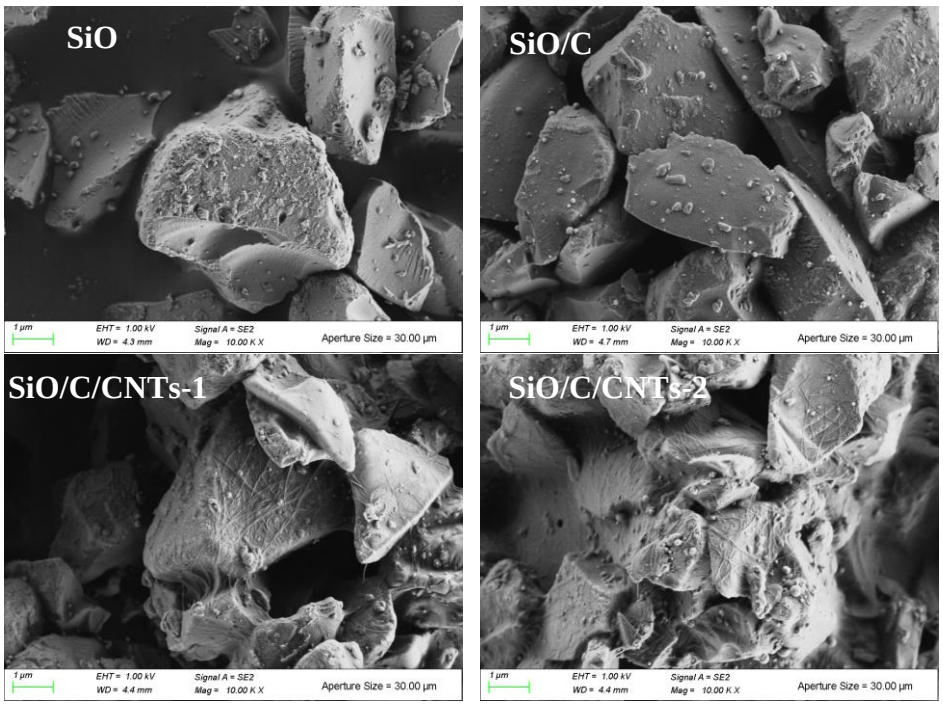

Figure 1. SEM of SiO, SiO/C, SiO/C/CNTs-1 and SiO/C/CNTs-2.

Fig. 2 shows the XRD curves of different samples. All samples have obvious amorphous SiO_2 diffraction peak and the carbon coated samples show obvious characteristic peaks of Si, which are due to the disproportionation reaction of SiO during the coating process, and in the formation of Si and SiO_2[22]. The crystallinity of SiO/C/CNTs-1 and SiO/C/CNTs-2 is better than SiO/C, indicating that the addition of carbon nanotubes are beneficial to form crystalline silicon. The diffraction peak of graphitic carbon does not appear, which indicates most of the carbon existence in amorphous.

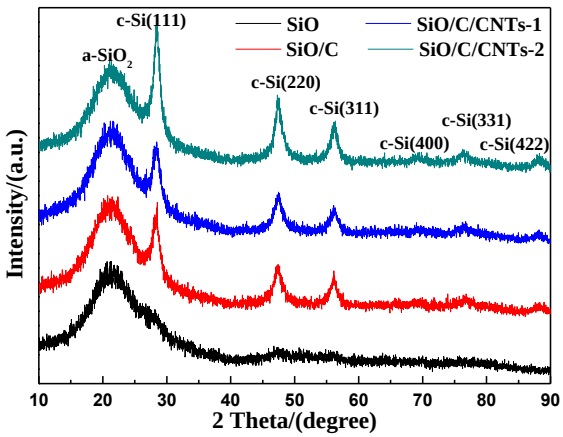

Figure 2. XRD curves of different samples.

Fig. 3 shows the Raman spectrum curves of different samples. The SiO has a broad peak at 465 cm^{-1}, which indicates the Si exists in the form of amorphous in the SiO[23]. The peaks of SiO/C,

SiO/C/CNTs-1 and SiO/C/CNTs-2 appear near 516cm^{-1}, 510cm^{-1} and 509cm^{-1}, respectively, which indicate obvious crystallization of Si, and the phenomena are consistent with the results of XRD analysis. After carbon coating, the peaks near 1350 cm^{-1} and 1590 cm^{-1} belong to D-band originated from the defective carbon atoms and G-band originated from the sp2 graphitic carbon atoms[24]. With the addition of carbon nanotubes I (G) /I (D) gradually increased, and the graphitization degree of the carbon coated increases accordingly.

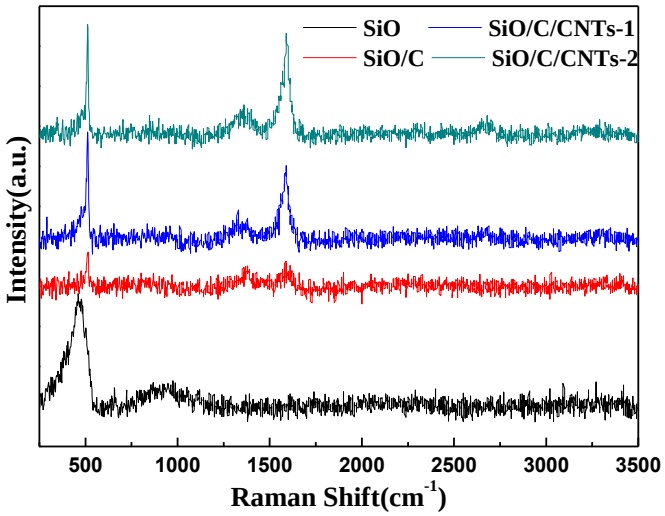

Figure 3. Raman spectrum curves of different samples.

Fig. 4 shows the initial charge-discharge curves of different samples at 0.1C. The SiO exhibits the highest initial charge-discharge capacity, which are 1601.6 mAh/g and 2268.3 mAh/g, and the lowest initial charge-discharge efficiency is 70.6%. Although the charge-discharge capacity of SiO decreased after carbon coating, and show a decreasing trend with the increase of the amount of carbon coating, but the initial charge-discharge efficiency of carbon coating samples are improved, as shown in table 1 and the maximum is 76.7% of SiO/C. The reason is that the carbon materials has a lower capacity and better electronic conductivity than SiO.Carbon coating hindered the reaction between electrolyte and SiO, improved the electronic conductivity of SiO and reduced the loss of lithium ions. The addition of carbon nanotubes does not significantly improve the initial charging-discharging capacity and initial coulomb efficiency of SiO, and the charging-discharging capacity decreased with the increase of the content of carbon nanotubes, which may be caused by the increase of the specific surface area of SiO/C/CNTs-1 and SiO/C/CNTs-2. BET specific surface area of all samples are shown in Table 2. In addition, carbon coating changes the initial intercalation potential of SiO, and the voltage profile is much closer to Si, which is consistent with the results of XRD analysis and Raman spectrum analysis[25].

Table 1. Initial charge-discharge parameters of different samples at 0.1C

Samples	SiO	SiO/C	SiO/C/CNTs-1	SiO/C/CNTs-2
Discharge/(mAh/g)	2268.3	2057.9	1925.9	1859.1
Charge/(mAh/g)	1601.6	1578	1464.6	1378.3
Coulombic efficiency/(%)	70.6	76.7	76.1	74.1

Table 2. BET specific surface area of different samples

Samples	SiO	SiO/C	SiO/C/CNTs-1	SiO/C/CNTs-2
BET/(m^2/g)	3.4127	20.4638	23.9765	27.0372

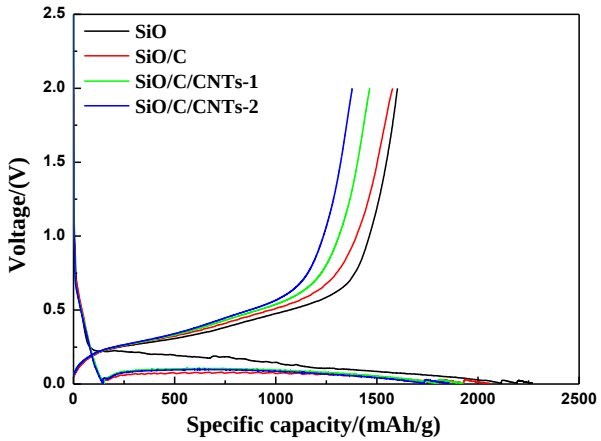

Figure 4. The initial charge-discharge curves of different samples at 0.1C.

Fig. 5 shows the charge-discharge cycle curves of different samples in the first five cycles at 0.1C. After 5 cycles, the charge capacity of SiO decreased significantly and the charge capacity of SiO/C reduced slighty. However the charge capacity of SiO/C/CNTs-1 and SiO/C/CNTs-2 added with carbon nanotubes increased with the boost in number of cycles.

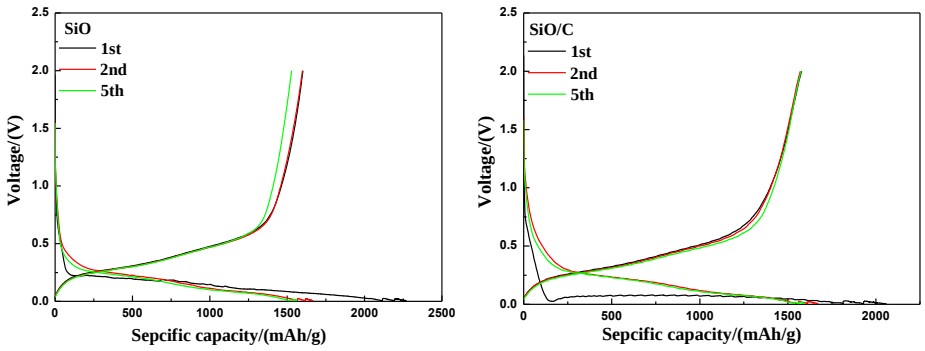

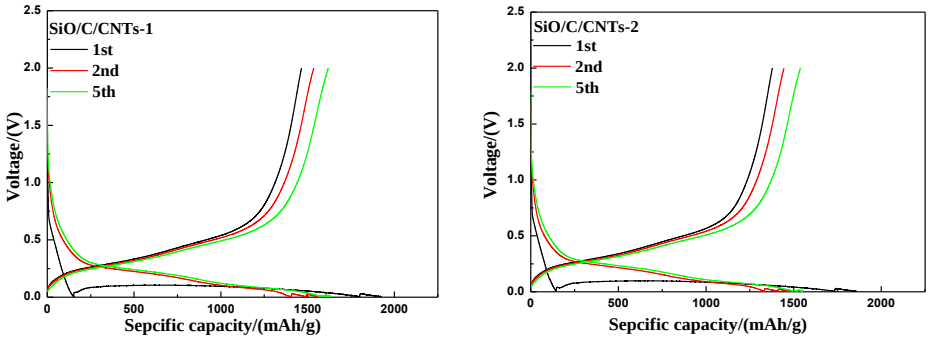

Figure 5. The charge-discharge cycle curves of different samples in the first five cycles at 0.1C.

This is attributed to SiO directly contacting with the electrolyte, and the SEI film formed is unstable which will break in the subsequent cycle and consumes more lithium ions, and reduces the capacity of SiO. While the SiO/C, SiO/C/CNTS-1 and SiO/C/CNTS-2 coated with carbon can form a carbon protective layer on the surface of SiO, which hinders the directly contact between SiO and electrolyte, and the expansion of SiO is inhibited. The hollow tubular structure and large specific surface area of carbon nanotubes enhance the electrolyte retention capability of the SiO, and build a good electronic conduction network, which are conducive to transport lithium ions and electrons.

All the samples undergo the first six cycles at 0.1C and then at 0.5C for the following cycles. Figure 6 shows the initial charge-discharge curves of different samples at 0.5C after the first six cycles at 0.1C. In contrast to the initial charge-discharge at 0.1C, SiO exhibits the lowest initial charge-discharge capacity at 0.5C, which are 1385.3 mAh/g and 1409.5 mAh/g. The SiO/C/CNTs-1 shows the highest initial charge-discharge capacity of 1603.4 mAh/g and 1593.8 mAh/g at 0.5C. The initial coulombic efficiency at 0.5C is the lowest of 98.3% for SiO and is the highest of 99.6% for SiO/C/CNTs-2. The initial charge-discharge parameters of different samples at 0.5C are shown in Table 3. The polarization of SiO is the most serious, which is due to the poor electronic conductivity and a bad SEI film formed. The carbon coating improves the electronic conductivity of SiO and a stable SEI film formed, which significantly improves the rate performance and dramatically decreases the polarization of SiO.

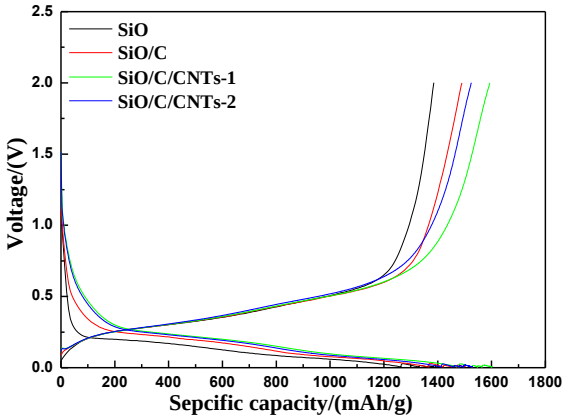

Figure 6. The initial charge-discharge curves of different samples at 0.5C after the first six cycles at 0.1C. .

Table 3. Initial charge-discharge parameters of different samples at 0.5C

Samples	SiO	SiO/C	SiO/C/CNTs-1	SiO/C/CNTs-2
Discharge/(mAh/g)	1409.5	1501.4	1603.4	1531.5
Charge/(mAh/g)	1385.3	1490	1593.8	1525
Coulombic efficiency/(%)	98.3	99.2	99.4	99.6

Table 4. Cycling performance of SiO-based anode for lithium ion batteries in recent reports

Samples	Reversible specific capacity	Current density (A/g)	Reference
SiO@F-doped C	752 mAh/g after 350 cycles	0.4	[24]
SiO/Ni/rGO	720 mAh/g after 100 cycles	0.1	[12]
SiO/@CNTs/C	821 mAh/g after 200 cycles	1	[22]
B-containing SiO_x	1186 mAh/g after 100 cycles	0.1	[23]
mp-SiO@N-doped C	806 mAh/g after 250 cycles	0.4	[15]
SiO@C/TiO_2	1565 mAh/g after 100 cycles	0.1	[13]
SiO/C/CNTs-2	1335 mAh/g after 114 cycles	0.85	this work

Fig. 7 shows the cycling curves of different samples in the first six cycles at 0.1C and then at 0.5C for the following cycles. The charge capacity of SiO decreased significantly in every cycle. The charge capacity of SiO is 1010.2 mAh/g after 20 cycles, the capacity retention rate is 63.1%, and the average cycle capacity loss is 29.6 mAh/g. The SiO/C declines obviously after 20 cycles, which exhibits charge capacity of 872.7 mAh/g, and the capacity retention rate is 55.3% after 120 cycles with an average cycle loss of 5.9 mAh/g. At the beginning of 0.1C and 0.5C cycles, SiO/C/CNTs-1 and SiO/C/CNTs-2 capacities increased with the number of cycle, and began to decline slowly after 15 cycles. After 120 cycles, SiO/C/CNTs-1 and SiO/C/CNTs-2 deliver the charge capacity of 1131.2 mAh/g and 1335.5 mAh/g, the capacity retention rate of 77.2% and 96.9%, and the average cycle loss of 2.8 mAh/g and 0.36 mAh/g. Table 4 compares the cycling performance of SiO-based anode for lithium ion batteries in recent reports with our work. Obviously, SiO/C/CNTs-2 shows a competitive performance in the long-term cycling stability.

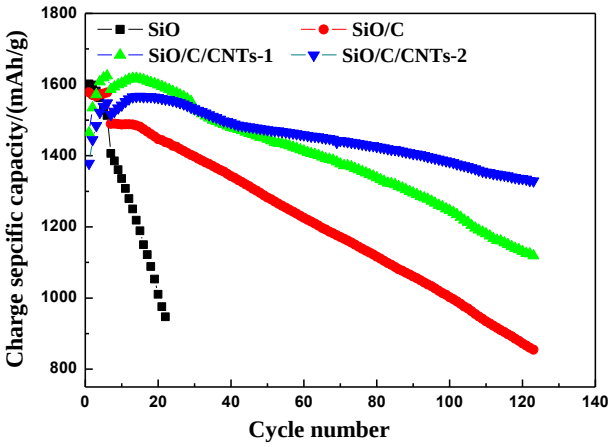

Figure 7. Cycling curves of different samples in the first six cycles at 0.1C and then at 0.5C for the following cycles.

4. CONCLUSIONS

The commercial SiO has low initial charge-discharge efficiency and poor cycle performance, which exhibits the capacity retention rate of 63.1% after 20 cycles. The maximum initial coulombic efficiency of SiO/C is 76.7% by coated vitamin C heated to 950℃, but the capacity retention rate is only 55.3% after 120 cycles, and the average cycle capacity loss is 5.9 mAh/g. The initial coulombic efficiency was increased and the cycling performance was improved significantly of commercial SiO by coated vitamin C and carbon nanotubes heated to 950℃. The prepared SiO/C/CNTs-2 delivered excellent performance, which are an initial charge-discharge efficiency of 74.1%, a high reversible capacity of 1335 mAh/g and a high retention rate of 96.9% after 120 cycles, and an low average cycle capacity loss of 0.36 mAh/g.

References

1. R. Yazami, P. Touzain, *J. Power Sources*, 9 (1983) 365.
2. H. J. Tian, X. J. Tan, F. X. Xin, C. S. Wang, W. Q. Han, *Nano Energy*, 11 (2015) 490.
3. N. Nitta, F. X. Wu, J. T. Lee, G. Yushin, *Materials today*, 18 (2015) 252.
4. M. N. Obrovac, L. J. Krause, *J. Electrochem. Soc*., 154 (2007) A103.
5. J. Yang, Y. Takeda, N. Imanishi, C. Capiglia, J. Y. Xie, O. Yamamoto, *Solid State Ionics*, 152 (2002) 125.
6. J. H. Kim, C. M. Park, H. Kim, Y. J. Kim, H. J. Sohn, *J. Electroanal. Chem*., 6 (2011) 245.
7. T. Huang, Y. X. Yang, K. C. Pu, J. X. Zhang, M. X. Gao, H. G. Pan, Y. F. Liu, *RSC Adv*., 7 (2017) 2273.
8. J. H. Kim, H. J. Sohn, H. S. Kim, G. J. Jeong, W. Choi, *J. Power Sources*, 170 (2007) 456.
9. X. Y. Wang, Z. Y. Wen, Y. Liu, X.G. Xu, J. Lin, *J. Power Sources*, 189 (2009) 121.
10. B. Liu, A. Abouimrane, Y. Ren, M. Balasubramanian, D. P. Wang, Z. G. Fang, K. Amine, *Chem. Mater.,* 24 (2012) 4653.
11. M. J. Zhou, M. L. Gordin, S. R. Chen, T. Xu, J. X. Song, D. P. Lv, D. H. Wang, *Eletrochem. Commun.*, 28 (2013) 79.

12. Y. Liu, J. Huang, X. Zhang, J. Wu, A. Baker, H. Zhang, S. Chang, X. Zhang, *J. Alloys Compd*., 749 (2018) 236.
13. L. Liu, X. X. Li, G. He, G. Q. Zhang, G. J. Su, C. H. Fang, *J. Alloys Compd*., 836 (2020) 155407.
14. B. C. Yu, Y. Hwa, J. H. Kim, H. J. Sohn, *Electrochim. Acta*, 117 (2014) 426.
15. X. Huang, M. Q. Li, *Appl. Surf. Sci*., 439 (2018) 336.
16. X. Q. Yuan, H. X. Xin, X. Y. Qin, X. J. Li, Y. F. Liu, H. F. Guo, *Electrochim. Acta*, 155 (2015) 251.
17. D. J. Lee, M. H. Ryou, J. N. Lee, B. G. Kim, Y. M. Lee, H. Kim, B. Kong, J. Park, J. W. Choi, *Electrochem. Commun*., 34 (2013) 98.
18. S. Komaba, K. Shimomura, N. Yabuuchi, T. Ozeki, H. Yui, K. Konno, *J. Phys. Chem*. C, 115 (2011) 13487.
19. X. J. Feng, J. Yang, X. L. Yu, J. L. Wang, Y. Nuli, *J. Soild State Electrochem*., 17 (2013) 2461.
20. L. B. Chen, K. Wang, X. H. Xie, J. Y. Xie, *J. Power Sources*, 174 (2007) 538.
21. N. Choi, K. H. Yew, K. Y. Lee, M. Sung, H. Kim, S. Kim, *J. Power Sources*, 161 (2006) 1254.
22. J. B. Li, L. Wang, F. M. Liu, W. J. Liu, C. K. Luo, Y.L. Liao, X. Li, M. Z. Qu, Q. Wan, G. C. Peng, *ChemistrySelect*, 4 (2019) 2918.
23. W. Yang, H. Liu, Z. H. Ren, N. Jian, M. X. Gao, Y. J. Wu, Y. F. Liu, H. G. Pan, *Adv. Mater. Interfaces*, 6 (2019) 1801631.
24. L. Z. Guo, H. Y. He, Y. R. Ren, C. Wang, M. Q. Li, *Chem. Eng. J*., 335 (2018) 32.
25. M. Mamiya, M. Kikuchi, H. Takei, *J. Cryst. Growth*, 237 (2002) 1909.